The core oligosaccharide component from *Mannheimia (Pasteurella) haemolytica* serotype A1 lipopolysaccharide contains L-*glycero*-D-*manno*- and D-*glycero*-D-*manno*-heptoses: Analysis of the structure and conformation by high-resolution NMR spectroscopy

Jean-Robert Brisson, Ellen Crawford, Dušan Uhrín, Nam Huan Khieu, Malcolm B. Perry, Wayne B. Severn, and James C. Richards

Abstract: Previous studies from our laboratory have indicated that the lipopolysaccharide (LPS) from *Mannheimia haemolytica* serotype A1 contains both L-*glycero*-D-*manno*-heptose and D-*glycero*-D-*manno*-heptose residues. NMR methods making use of 1D ^{1}H selective excitation and 2D (^{1}H, ^{13}C) and (^{1}H, ^{31}P) heteronuclear experiments were used for the structural determination of the major core oligosaccharide components of the deacylated low-molecular-mass LPS obtained following sequential treatment with anhydrous hydrazine and aq KOH. The core oligosaccharide region was found to be composed of a branched octasaccharide linked to the deacylated lipid A moiety via a 3-deoxy-4-phospho-D-*manno*-oct-2-ulosonate residue having the structure,

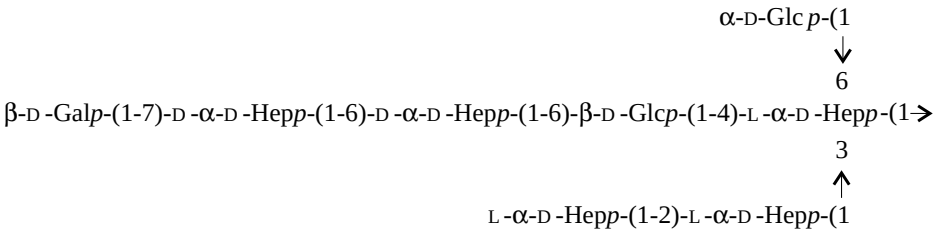

Heterogeneity was found to be present at several linkages. NMR methods were devised to distinguish between the diastereomeric forms of the heptose residues. Synthesized monosaccharides of L-D- and D-D-heptose were used as model compounds for analysis of the ^{1}H and ^{13}C NMR chemical shifts and proton coupling constants. Molecular modeling using a Monte Carlo method for conformational analysis of saccharides was used to determine the conformation of the inner core of the oligosaccharide and to establish the stereochemical relationships between the heptoses.

Key words: LPS, NMR, conformation, oligosaccharide, heptose.

Résumé : Des études antérieures effectuées dans notre laboratoire ont indiqué que le lipopolysaccharide (LPS) obtenu à partir de *Mannheimia haemolytica* sérotype A1 contient des résidus de L-*glycéro*-D-*manno*-heptose ainsi que de D-*glycéro*-D-*manno*-heptose. On a utilisé des méthodes de RMN faisant appel à l'excitation selective du ^{1}H en 1D et à des expériences hétéronucléaires (^{1}H,^{13}C) et (^{1}H,^{31}P) en 2D pour déterminer la structure des composants oligosaccharides principaux du noyau du LPS désacétylé, de faible masse moléculaire, obtenu après un traitement séquentiel avec de l'hydrazine anhydre et du KOH aqueux. On a trouvé que l'oligosaccharide de la région du noyau est formée d'un

Received 10 January 2002. Published on the NRC Research Press Web site at http://canjchem.nrc.ca on 5 August 2002.

Dedicated to the memory of Professor Raymond U. Lemieux who pioneered the applications of NMR spectroscopy for stereochemical and conformational analyses of carbohydrates.

J.-R. Brisson, E. Crawford, N.H. Khieu, M.B. Perry, and J.C. Richards.[1] Institute for Biological Sciences, National Research Council, Ottawa, ON K1A 0R6, Canada.
W.B. Severn. Agricultural Research, Department of Diseases, PO Box 40063, Ward Street, Upper Hutt, New Zealand.
D. Uhrín. University of Edinburgh, Department of Chemistry, West Mains Road, Edinburgh EH9 3JJ, U.K.

[1]Corresponding author (e-mail: jim.richards@nrc.ca).

 DOI: 10.1139/V02-114

oligosaccharide ramifié lié à une portion désacétylée du lipide A par le biais d'un résidu 3-désoxy-4-phospho-D-*manno*-oct-2-ulosonate de structure,

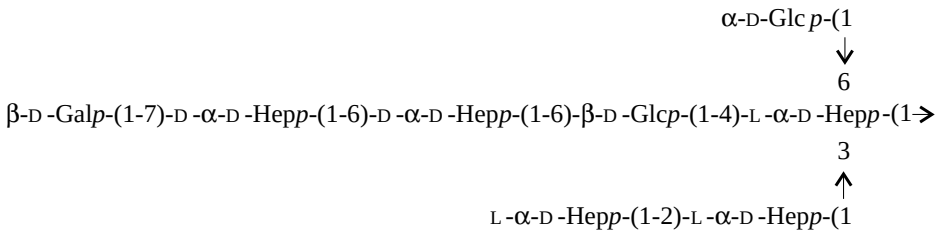

On a observé de l'hétérogénéité à plusieurs points de ramification. On a mis au point des méthodes RMN qui permettent de faire la différence entre les formes diastéréomères des résidus heptoses. On a utilisé des monosaccharides de synthèse de L-D- et D-D-heptoses comme modèles pour l'analyse des déplacements chimiques du ^{1}H et du ^{13}C et des constantes de couplage du proton. On a utilisé la modélisation moléculaire basée sur la méthode de Monte Carlo pour faire l'analyse conformationnelle des saccharides afin déterminer la conformation du noyau de l'oligosaccharide et établir les relations stéréochimiques entre les heptoses.

Mots clés : LPS, RMN, conformation, oligosaccharide, heptose.

[Traduit par la Rédaction]

Introduction

Lipopolysaccharides (LPS) are a complex class of glycolipids that can trigger a cascade of immunological responses in mammals including endotoxic effects and serum antibody production (1). These molecules make up the outer leaflet of the outer membrane of Gram-negative bacteria. LPS has been found to exhibit a common molecular architecture consisting of at least two distinct regions: (*i*) an oligo- or polysaccharide region; and (*ii*) a lipid moiety referred to as lipid A (2). In certain bacteria, the carbohydrate containing region consists of a high-molecular-mass *O*-specific polysaccharide, which is covalently linked to a core oligosaccharide unit (3). Other bacteria, notably *Haemophilus* and *Neisseria s*pp. only produce short-chain LPS, devoid of *O*-polysaccharide chains, in which the carbohydrate region contains mixtures of low-molecular-mass but structurally diverse oligosaccharide components. The saccharide portion of LPS molecules has been found to be linked to the lipid A moieties via the eight-carbon sugar acid, 3-deoxy-D-manno-oct-2-ulosonate (Kdo). The lipid A from several bacterial species has been found (2) to have a relatively conserved structure consisting of a bisphosphorylated β-1,6-linked D-glucosamine (GlcN) disaccharide unit that is substituted by fatty acyl amide and ester groups.

The bacterium *Mannheimia haemolytica* is a new member of the Pasteurellaceae family (4). Originally referred to as *Pasteurella haemolytica*, this group of organisms was classified into two biotypes (designated A and T) which were further subdivided into 17 serotypes (5, 6). This biochemical distinction was based on the ability of the organisms to ferment either arabinose (A-biotype) or trehalose (T-biotype) (7). On the basis of genetic analyses, the *P. haemolytica* biotype T organisms (serotypes T3, T4, T10, and T15) were reclassified as *Pasteurella trehalos* in 1990 (8, 9). More recently the biotype A group of organisms was reclassified into the new genus *Mannheimia* (10). Twelve *M. haemolytica* serotypes are now recognized (A1, A2, A5, A6, A7, A8, A9, A12, A13, A14, A16, and A17). *M. haemolytica* serotype A1 is most frequently associated with bovine pneumonic pasteurellosis (shipping fever), a major cause of sickness and economic loss to the feed lot industry (11, 12). The pathogenesis of diseases caused by *M. haemolytica* in cattle has recently been reviewed (13). Several virulence factors, including a leukotoxin, capsular polysaccharide, and LPS have been identified. *M. haemolytica* LPS has been reported to have a severe damaging effect on bovine endothelial cells (14, 15).

In our laboratory we have undertaken the structural and antigenic characterization of *M. haemolytica* (16, 17) and *P. trehalos* (17–20) LPS to understand the role of these molecules in pathogenesis and protective immunity. Immunochemical studies have revealed that eight of the 12 *M. haemolytica* serotypes can elaborate LPS which contain a common *O*-polysaccharide side chain (17). The structure of the *O*-polysaccharide from serotype A1 is representative and was determined in detail. It consists of a trisaccharide repeating unit having the structure -4)-β-D-Gal*p*-(1–3)-β-D-Gal*p*-(1–3)-β-D-Gal*p*NAc-(1- (16). A detailed structural model for the core oligosaccharide of *M. haemolytica* LPS serotype A1 core oligosaccharide has not been proposed.

Many carbohydrate samples of biological origin are heterogeneous in nature and difficult to separate. To determine their three-dimensional structure, complete NMR assignments are desirable even for heterogeneous products. Only then can conformational analysis (21) be made with the goal of establishing a relationship between three-dimensional structure and biological function (22). Towards this goal, 1D selective NMR methods have been used to determine the structure of mixtures, where the resonances of specific components can be selected to characterize individual components (23–28). 1D selective excitation experiments are analogs of standard 2D and 3D experiments where hard pulses have been replaced by selective pulses. The original phase-cycled experiments (29–42) have more recently been adopted for the use of pulsed-field gradients (43–55). Particularly useful are 1D analogues of 3D experiments (53–55).

Fig. 1. Proton NMR spectrum at 600 MHz of the core oligosaccharide component from *M. haemolytica* serotype A1 LPS in D_2O (300 K, pH 3). The HOD resonance is at 4.756 ppm. Resonances in the anomeric region up from 4.4 ppm are labelled along with the Kdo methylene resonances. The determined structure designated as A1 and nomenclature for the residues are also shown. Heterogeneity due to partial truncation of the backbone oligosaccharide is indicated by dotted arrows at linkage sites. In the text, the minor component for f due to heterogeneity is indicated by f′. Hep_I, Hep_{II}, and Hep_{III} are L-D-heptose while Hep_{IV} and Hep_V are D-D-heptoses. Other residues have the D-configuration.

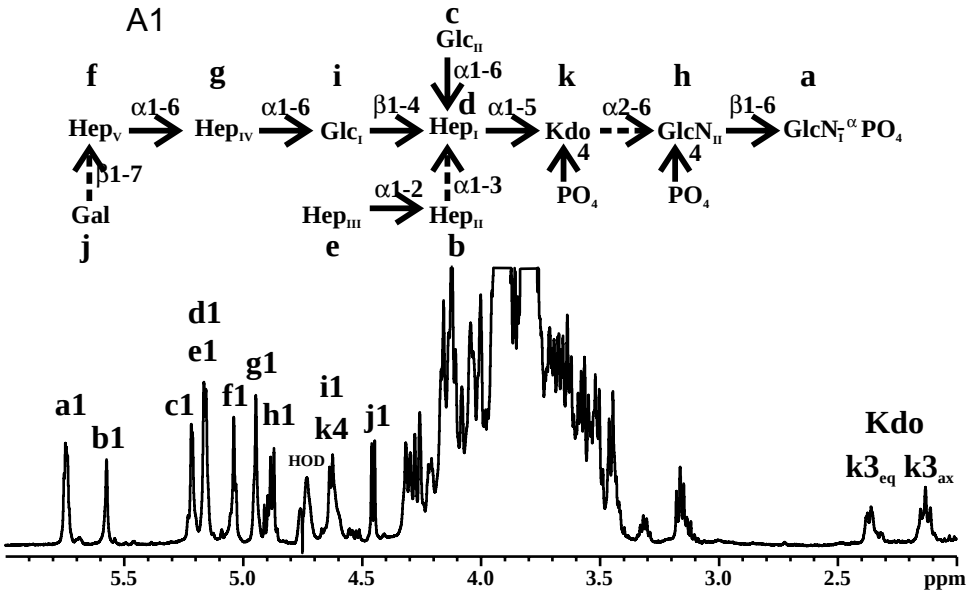

An advantage of 1D selective methods is that the multiplet pattern for each resonance in the 1D selective experiments can be clearly observed due to the same digital resolution as a 1D ^1H spectrum. Also, 1D selective experiments are sometimes preferable to 2D methods for the structural analysis of oligosaccharides as was recently demonstrated in the characterization of some enzymatically synthesized oligosaccharides (56, 57). Also, with selective experiments, incursion in the ring region of carbohydrates is possible. The 1D TOCSY-NOESY permits the isolation of spin systems of interests and the detection of NOEs from proton resonances within the ring allowing NOE constraints to be obtained which cannot be otherwise determined from 2D experiments (58, 59). Recently several reviews have dealt with carbohydrate structural determination by NMR spectroscopy (60–64).

Preliminary studies by chemical, ^1H NMR, and mass spectrometric (MS)-based methods have indicated that the LPS core region of *M. haemolytica* A1 has the composition $Hex_{2-3}Hep_5Kdo$. The Hex_2Hep_5Kdo species is the major core oligosaccharide component in the *O*-chain deficient serotype A8 LPS (17). Analyses of the LPS from these serotypes indicate the core oligosaccharide to contain D-glucose, D-galactose and both L-glycero-D-manno-heptose (L-D-heptose) and D-glycero-D-manno-heptose (D-D-heptose) residues. In the present investigation the structure of the core oligosaccharide of *M. haemolytica* serotype A1 LPS was determined in detail. The sequence, linkage positions, and relative stereochemistries of the heptose-containing oligosaccharide were established by NMR spectroscopic techniques. On the basis of NMR analyses and Monte Carlo calculations a conformational model is now proposed for the core oligosaccharide region of the LPS.

Results and discussion

Our previous analysis of the LPS of *M. haemolytica* serotype A1 revealed Hex_3Hep_5Kdo as the major core oligosaccharide component. This was determined by 1D ^1H NMR and FAB-MS analysis of the oligosaccharide fraction obtained following mild acid hydrolysis (1% HOAc, 100°C, 3 h) of the LPS sample (17). The core oligosaccharide was found to contain D-glucose, D-galactose, L-D-heptose, and D-D-heptose in a molar ratio of 2:1:3:2 in the major fraction as determined by GLC–MS analysis of their alditol acetate and 2-butyl glycoside derivatives. The D-Gal residue was found to be a terminal nonreducing moiety from methylation analysis and was absent in the minor component of the core oligosaccharide fraction, that had the composition of Hex_2Hep_5Kdo. The occurrence of Kdo in the LPS was established by colorimetric analysis.

Treatment of *M. haemolytica* LPS with anhydrous hydrazine followed by strong alkali afforded water-soluble, deacylated LPS oligosaccharides. The deacylated LPS sample was representative of the intact backbone oligosaccharide of the native material containing core and lipid A oligosaccharide moieties. This was confirmed by electrospray ionization ESI-MS which gave molecular ions corresponding to $Hex_3Hep_5Kdo_1HexN_2(H_2PO_3)_3$ as the major oligosaccharide component (see *Experimental section*).

From the proton spectrum (Fig. 1) and HMQC and COSY spectra (Fig. 2), 10 anomeric ^1H NMR resonances were observed, as well as methylene proton resonances. The anomeric resonances were labeled a–j in decreasing order of their ^1H NMR chemical shifts and $k3_{eq}$ and $k3_{ax}$ assigned to the methylene protons of Kdo. The integral for the b1 and de1 and j1 anomeric peaks were 40% less than those for the

Fig. 2. 2D NMR experiments for A1 showing the HMQC spectrum of the anomeric region (*a*), and the COSY (*b*) and NOESY (*c*) spectra of the anomeric and ring region. The arrow indicates the position of the b2 resonance observed near k5.

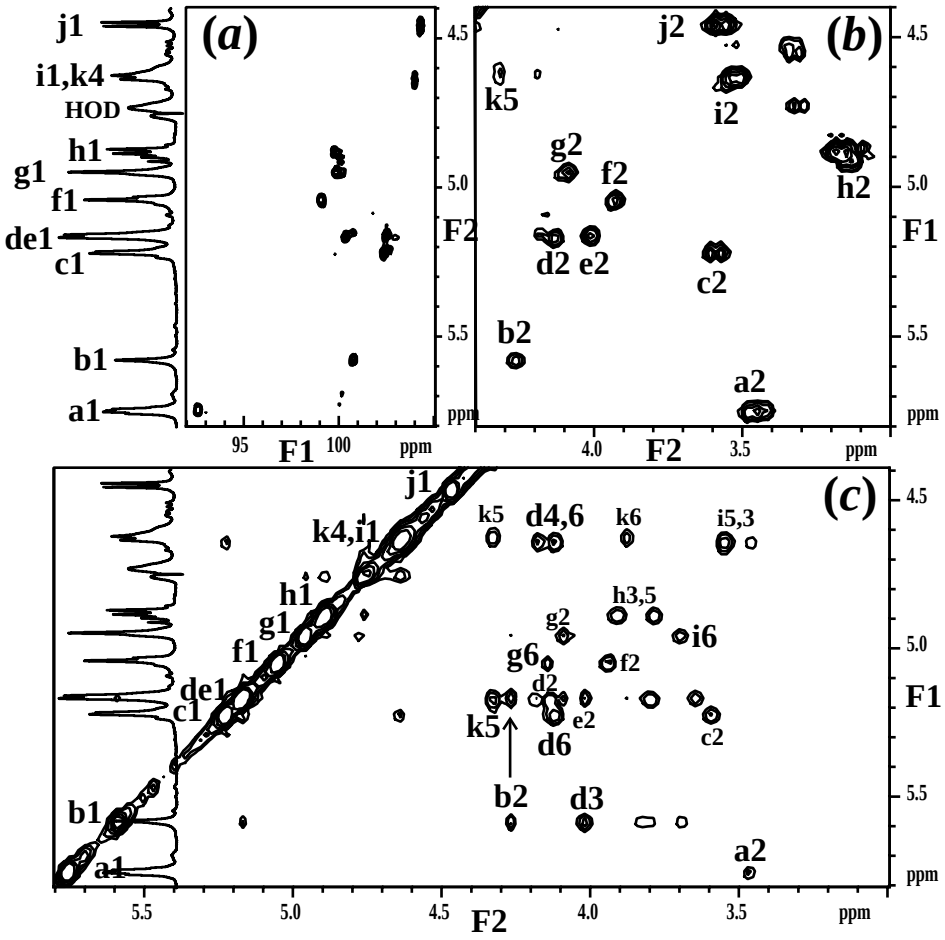

other anomeric resonances confirming heterogeneity in the sample. There was also some heterogeneity at h1 with the appearance of a downfield doublet at 4.91 ppm near h1.

Standard homo- and hetero-nuclear 2D-NMR analyses was undertaken. From the COSY spectrum in Fig. 2, the H-2 resonances could be located. It was realized that for residues **b**, **d**, **e**, **f**, and g, $J_{1,2}$ was small, typical of *manno*-heptoses, and that a 2D-TOCSY could not be used to transfer magnetization from H-1 past H-2. From the HMQC spectrum in Fig. 3, the H-2 of the heptose residues overlapped with other resonances making 2D-TOCSY difficult to analyze for these residues. The 2D-NOESY spectrum also showed an unusually high number of NOEs especially for the b1, de1 resonances. Also, there was overlap of several resonances in the anomeric region. Hence, due to the complexity of the spectra and heterogeneity of the sample, 1D selective methods were used to extract spectral parameters that could not be obtained using standard 2D methods, thus permitting the resolution of the structure and conformational analysis. HMQC-TOCSY and HMBC experiments were also very important in determining the complete assignments, especially for the heptose units. Using this approach, the complete assignment for the ^{1}H and ^{13}C NMR chemical shifts for the major backbone oligosaccharide (A1) was possible (Table 1).

The Kdo-$GlcN_{II}$-$GlcN_{I}$ sequence and partial assignments are known from previous studies (65) and are consistent with the assignments made here. The 1D-TOCSYs for residues **a** and **h** permitted assignment of the resonances and measurement of proton coupling constants (Fig. 4*a*, 4*b*). Location of phosphate groups was confirmed from a ^{31}P HMQC experiment as done previously (65). Assignment of the ^{13}C NMR chemical shifts was then made from HMQC, HMQC-TOCSY, and HMBC spectra. This information led to the definition of residues **a** and **h** as the α-D-GlcN and β-D-GlcN pyranosyl units of the lipid A moiety. Most of the proton, ^{31}P and ^{13}C NMR chemical shifts were similar to those previously reported in a similar structural element (65). In the 1D-TOCSY for h1, the h′5 peak at 3.62 ppm is due to hydrolysis of the Kdo-(2-6)-β-D-$GlcN_{II}$ glycosidic linkage. After several months in solution, the linkage was completely hydrolyzed with h′6 and h′6 appearing at 3.82 and 3.92 ppm, respectively. The sharp anomeric signal at 3.91 ppm was also found to be due to h′1 of this disaccharide.

For Kdo, the H-4 and H-5 resonances were assigned from 1D-TOCSY experiments with selective excitation of H-3_{eq} or H-3_{ax}. The H-4 resonance is shifted downfield due to a phosphate group at C-4, confirmed by a ^{31}P HMQC. A small $J_{5,6} < 1$ Hz impeded the TOCSY transfer past H-5 (Fig. 4*c*). However, a strong NOE is observed between k4 and k6 in Fig. 2*c* in accord with the X-ray structure of Kdo (66). 1D NOESY-TOCSY(k4, k6) was used to complete the assignment

Fig. 3. Selected plots from the heteronuclear ^{1}H-^{13}C 2D NMR spectra of A1. (*a*) In the HMQC spectrum of the ring region some assignments are labelled where possible. (*b*) In the HMQC-TOCSY spectrum, the C7-H7s-C6-H6, C4-H4-C5-H5 TOCSY correlations and those for b2 are labelled. (*c*) In the HMBC spectrum, the H1-C1-O1-C*x* inter-glycosidic correlations are shown for the anomeric proton resonances along with their intra-residue correlations.

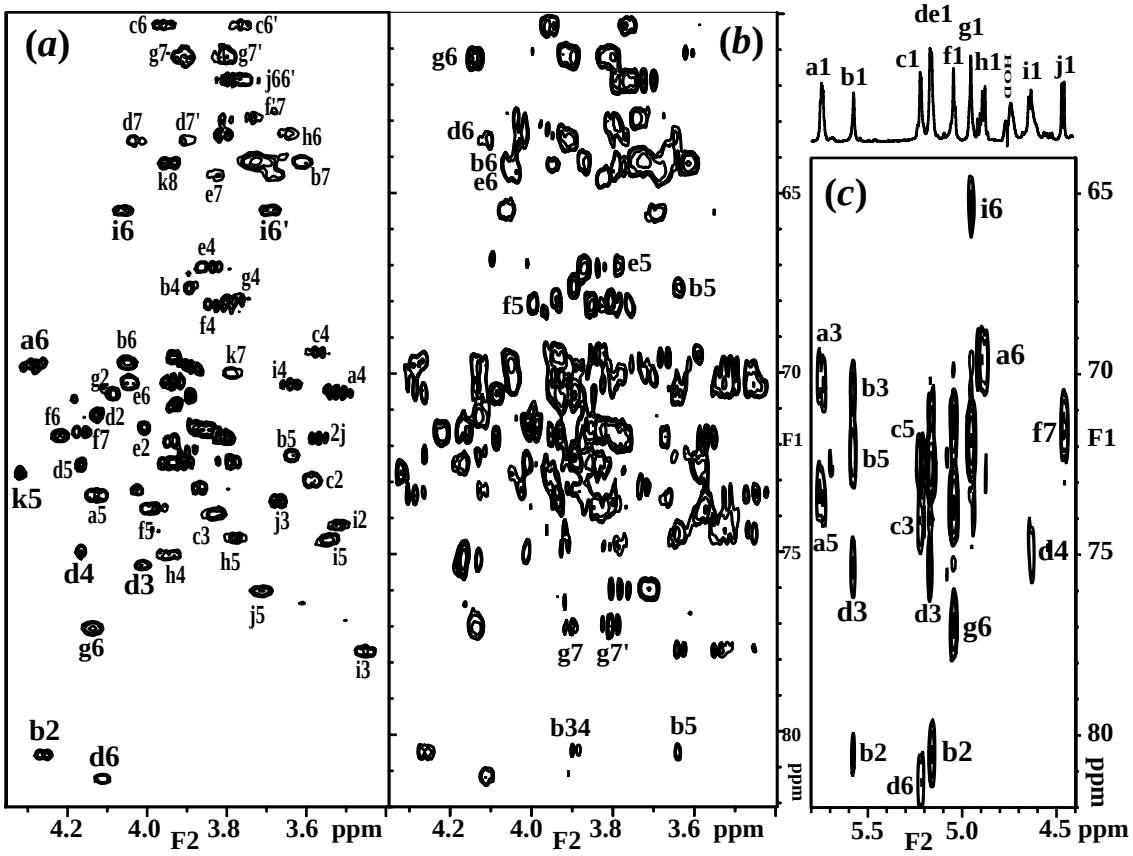

(Fig. 4*d*). As shown later, for the HepI-(1-5)-Kdo linkage, the d1-k7 NOE was also observed, typical of a substitution at C-5 of Kdo (67). Using this NOE, the Kdo resonances detected from the 1D-NOESY-TOCSY (de1, k7) (Fig. 4*e*) had the same chemical shifts and similar multiplet patterns as those found in the previous experiment, thus confirming the Kdo ^{1}H NMR assignments. The ^{13}C NMR assignments for Kdo where then obtained from the HMQC spectrum and confirmed from the HMQC-TOCSY spectrum.

Residue **i** was determined to be 6-substituted β-D-glucose denoted as Glc_I. The anomeric resonance for residue **i** overlapped with the H-4 resonance of Kdo. In the 1D-TOCSY for these two overlapping resonances, it was possible to distinguish the resonances for residue **i** because of the small $J_{5,6}$ coupling constant for Kdo (Fig. 4*c*). All resonances up to H-6s could be detected and coupling constants of the multiplets could be measured. Due to its β-D configuration the i1-i3 and i1-i5 NOE were also observed in the NOESY spectrum (Fig. 2 and Fig. 5*f*). ^{13}C NMR assignments for Glc_I were then obtained from the HMQC spectrum and confirmed with the HMQC-TOCSY spectrum. From a comparison with chemical shifts of terminal glucose (68, 69), a glycosidation down-field shift of 3.7 ppm was observed for the C-6 resonance, indicating its substitution at that position. A substantial shift of –2.2 ppm was also observed for C-5. The rotamer distribution about the C-5—C-6 bond could be determined from the H-5 multiplet observed for the i1-i5 NOE in Fig. 5*f*. It was apparent that both $J_{5,6}$ and $J_{5,6'}$ had small values <2 Hz since the H-5 multiple appeared as a doublet dominated by the large $J_{4,5}$ coupling of 10 Hz. This showed that both H-6 and H-6′ were gauche to H-5 with the O6-C6-C5-O5 = –60° rotamer being preferred in solution.

Residue **c** was determined to be a terminal α-D-glucose denoted as Glc_{II}. From the 1D-TOCSY for c1 (Fig. 4*f*) resonances up to H-5 were detected, indicating that residue **c** was an α-glucose based on the measured proton coupling constants. From the HMQC spectra and comparison with chemical shifts of terminal glucose model compounds (68, 69), all the ^{1}H and ^{13}C NMR assignments could be completed.

The terminal galactose, residue **j**, denoted as Gal, was identified from the 1D-TOCSY of j1 and resonances up to H-4 were observed (Fig. 4*j*). To get past the small $J_{4,5}$ coupling constants and identify H-5, the 1D-TOCSY-NOESY (j1, j4) was done (Fig. 4*h*). From the HMQC spectra and comparison with chemical shifts of terminal galactose model compounds (68, 69), all the ^{1}H and ^{13}C NMR assignments were completed.

To assign the heptose residues, model compounds were synthesized to obtain accurate ^{1}H and ^{13}C NMR chemical shifts and $J_{H,H}$ values. These were crucial in assigning the terminal heptose units by chemical shifts comparisons. Also,

Table 1. NMR chemical shifts (ppm) of the core oligosaccharide component from *Mannheimia* (*Pasteurella) haemolytica* serotype A1 LPS.

Residue	δ_C δ_H	C-1 H-1	C-2 H-2	C-3 H-3 H-3′	C-4 H-4	C-5 H-5	C-6 H-6 H-6′	C-7 H-7 H-7′	C-8 H-8 H-8′
Hep_I		100.3	71.1	75.3	74.9	72.5	81.2	63.5	
D		5.17	4.13	4.01	4.17	4.17	4.11	4.02	
								3.89	
Hep_{II}		100.7	80.5	70.6	67.6	72.2	69.6	64.1	
B		5.57	4.26	3.89	3.90	3.64	4.05	3.70	
								3.60	
Hep_{III}		102.5	71.5	71.5	67.0	72.4	70.2	64.5	
E		5.16	4.01	3.87	3.83	3.78	4.04	3.83	
								3.68	
Hep_{IV}		99.8	70.5	71.7	67.9	71.8	77.0	61.2	
G		4.95	4.08	3.81	3.78	3.94	4.14	3.91	
								3.80	
Hep_V		99.0	70.8	71.5	68.1	73.7	71.7	71.6	
F		5.04	3.93	3.85	3.82	3.99	4.22	4.16	
								3.85	
Hep_V		99.0	70.8	71.5	68.3	73.7	72.8	62.9	
f′		5.04	3.93	3.85	3.77	3.97	4.05	3.79	
								3.73	
Glc_I		104.0	74.2	77.7	70.2	74.6	65.5		
I		4.64	3.51	3.45	3.64	3.54	4.06		
							3.69		
Glc_{II}		102.4	72.9	73.9	69.3	72.4	60.3		
C		5.22	3.58	3.83	3.58	3.95	3.96		
							3.76		
Gal		104.3	71.7	73.5	69.5	76.0	61.8		
J		4.46	3.56	3.67	3.93	3.71	3.80		
							3.76		
$GlcN_I$		92.6	54.8	70.2	70.5	73.4	69.7		
A		5.75	3.45	3.93	3.51	4.13	4.28		
							3.89		
$GlcN_{II}$		99.7	56.3	72.2	75.0	74.6	63.4		
H		4.88	3.17	3.90	3.94	3.78	3.81		
							3.64		
Kdo			99.7	34.5	70.8	72.7	73.2	69.9	64.2
K				2.37	4.61	4.32	3.87	3.78	3.94
				2.13					3.73

Note: Measured at 600 MHz (^{1}H) in D_2O, 25°C and pH 3 from HMQC and HMBC data with the CH_3 signal of external acetone set at 2.225 ppm for ^{1}H NMR and 31.07 ppm for ^{13}C NMR. Average error of ±0.2 ppm for δ_C and ±0.02 ppm for δ_H. The minor component for f due to heterogeneity is indicated by f′. The CH_2 spin systems, (H, H′), are in decreasing order of chemical shifts. For Kdo, H-3 and H-3′ are assigned to H-3_{eq} and H-3_{ax}.

upon glycosidation, the ^{13}C NMR resonance of the substituted carbon experiences a substantial down-field glycosidation shift (56, 57). The proton spectra for D-D-heptose and D-L-heptose are shown in Fig. 6. In solution both the α and β forms are present for each compound. Their ^{1}H NMR spectra were assigned using 1D-TOCSY experiments. To obtain accurate coupling constants and chemical shifts, spin simulations of the proton spectra were done. The simulated spectra are shown in Fig. 6. The simulated spectra reproduced exactly the observed spectra, especially the strong coupling for H-3-H- in D-α-L-heptose (Fig. 6*b*). ^{13}C NMR chemical shifts were assigned using HMQC. The NMR data for the heptose monosaccharides are given in Table 2. The chemical shifts for L-D-heptose are the same as those of D-L-heptose since they are enantiomers of each other.

Residues **b**, **d**, **e**, **f**, and **g** in A1 were identified as heptoses from their narrow anomeric resonance due to the small $J_{1,2}$ coupling and lack of transfer of magnetization beyond H-2 from H-1 in a TOCSY experiment. All the heptoses in A1 had the α-D configuration since the only intra-residue NOE from H-1 was to H-2 (Fig. 2). 1D-TOCSY-TOCSY (H-1, H-2) was used to assign all the heptose residues. The first TOCSY step from H-1 transfers the magnetization to H-2 and further transfer is impeded due to the small $J_{1,2}$ value of 1.8 Hz. However, the second step at H-2 will transfer the magnetization further to higher spins due to the larger $J_{2,3}$ value of 3 Hz. However, for L-D-heptose, transfer of magnetization stops at H-5 due to the small $J_{5,6}$ value of 1.6 Hz. For D-D-heptose, transfer of magnetization is less impeded due to a large $J_{5,6}$ value of 3.2 Hz. However, relaxation

Fig. 4. 1D selective experiments for assignment of the non heptose residues in A1. (*a*) 1D TOCSY (a1, 180 ms); (*b*) 1D TOCSY (h1, 180 ms); (*c*) 1D TOCSY (i1 k4, 180 ms); (*d*) 1D NOESY-TOCSY (i1 k4, 400 ms; k6, 180 ms); (*e*) 1D NOESY-TOCSY (de1, 400 ms; g3 k7, 180 ms); (*f*) 1D TOCSY (c1, 180 ms); (*g*) 1D TOCSY (j1, 180 ms); and (*h*) 1D TOCSY-NOESY (j1, 180 ms; j4, 400 ms). Minor components for f and h due to heterogeneity are indicated by f′ and h′, respectively. The resonance for the first selective step is underlined and the one for second selection step is doubly underlined, where applicable. Selected resonances in the anomeric region are indicated on the left of the spectra.

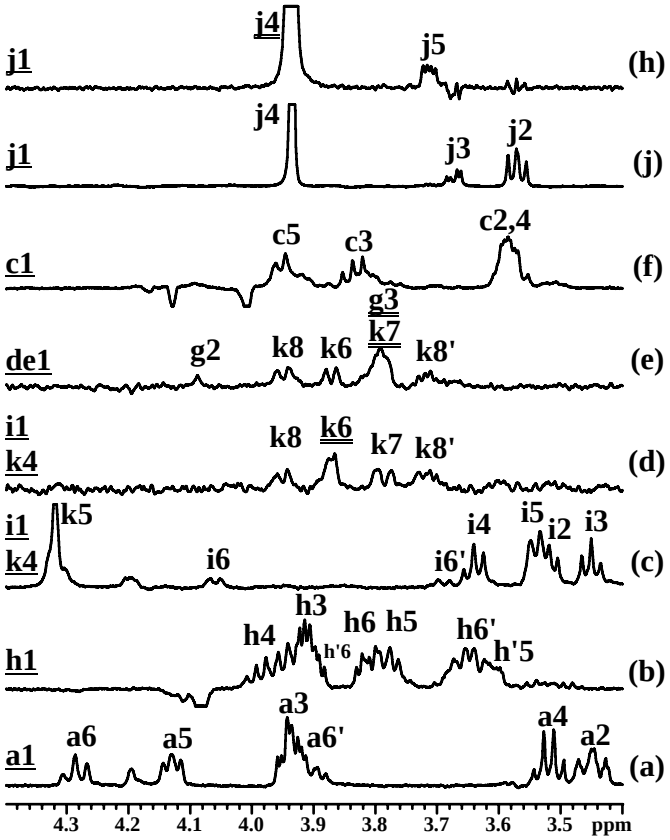

effects can also impede transfer of magnetization and one cannot use a lack of transfer beyond H-5 as proof of L-D-heptose identification.

Residue **b** was determined to be the 2-substituted L-α-D-heptose denoted as Hep_{II}. The 1D-TOCSY-TOCSY (b1, b2) identified resonances at 3.64 ppm and 3.9 ppm (Fig. 7*a*). The multiplet pattern at 3.64 ppm was indicative of a H-5 resonance while those at 3.9 ppm were similar to the strongly coupled H-3 and H-4 resonances observed in the monosaccharide (Fig. 6*b*). To identify H-6 a 1D-TOCSY-NOESY (b2, b5) was done (Fig. 7*b*). In the first TOCSY step for b2, the a6 resonance was also irradiated but the second step only selected the b5 resonance. NOEs from b2 were observed on b3 and b6 along with an inter-residue NOE on d2. Once b6 was located, the HMQC-TOCSY from the C-7-H-7s-C-6-H-6 was used to assign the H-7 and H-7′ resonances (Fig. 3*b*). Assignments for the other resonances were then obtained from the HMQC spectrum and confirmed from the HMQC-TOCSY and HMBC spectra

Fig. 5. 1D selective experiments to detect dipolar interactions in A1. 1D NOESY spectra of the resonances in the anomeric region with a 200 ms mixing time for b1, c1, de1, f1, g1, i1/k4 and a 1D ROESY (f1, 500 ms) for j1 in (*a*)–(*g*), respectively. The selected anomeric resonances and the linkage are indicated on the left of the spectra.

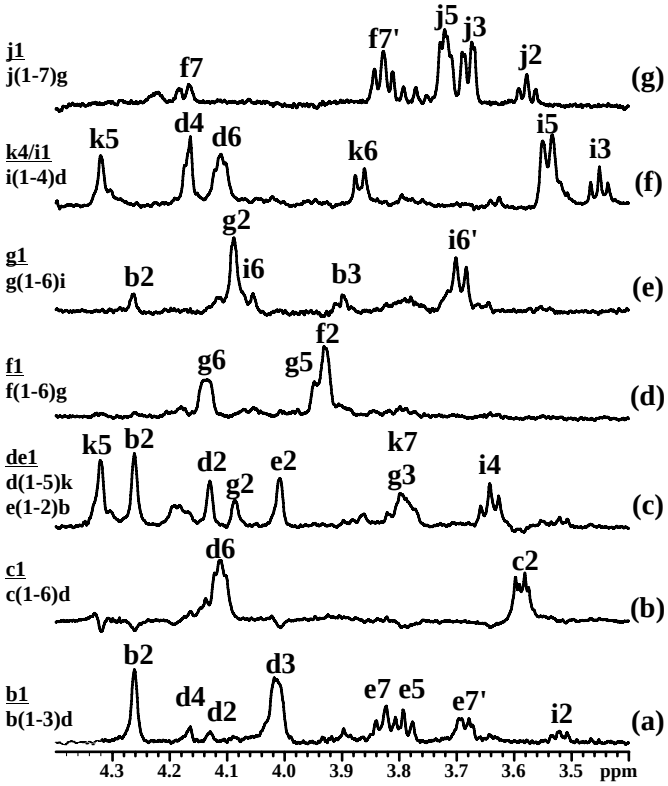

(Fig. 3). Comparison of chemical shifts with those of L-α-D-heptose indicated a 9 ppm down-field shift for C-2 and an up-field shift of –0.8 ppm for C-3 indicative of a substitution at C-2. The C-4 to C-7 chemical shifts were within 0.6 ppm of those of the monosaccharide.

Residue **e** was determined to be a terminal L-α-D-heptose denoted as Hep_{III}. Although the d1 and e1 resonances overlap, this is of no concern since their H-2 resonances did not overlap. The 1D-TOCSY-TOCSY (de1, e2) identified the e3, e4, and e5 spins (Fig. 7*c*). From the b1 NOE in Fig. 5*a*, the e5 resonance was also observed. The high digital resolution of the 1D selective experiments permits accurate matching of resonances between different experiments due to the observation of their multiplet pattern. In Fig. 5*a*, the b1-e7 and b1-e7′ NOEs were also observed. As seen later, these NOEs are due to the close proximity of b1 proton to the e5 and the e7 and e7′ protons. The H-6 resonance was located in the HMQC-TOCSY from C-7-H-7s-C-6-H-6. ^{1}H and ^{13}C NMR assignments were completed with HMQC and HMQC-TOCSY. ^{1}H and ^{13}C NMR chemical shifts of residue **e** were similar to those of L-α-D-heptose.

Residue **d** was identified as a 3,4,6-trisubstituted L-α-D-heptose denoted as Hep_{I}. The 1D-TOCSY-TOCSY (de1, d2) identified a narrow multiplet at 4.17 and a broader one at 4.01 ppm (Fig. 7*d*). The multiplets at 4.01 ppm and 4.17 ppm (d2) were also observed in the 1D-NOESY for b1 (Fig. 5*a*). The resonance at 4.17 ppm was also observed in

Table 2. NMR data for D-L-heptose and D-D heptose monosaccharides.

	δ_C	C-1	C-2	C-3	C-4	C-5	C-6	C-7	
	δ_H	H-1	H-2	H-3	H-4	H-5	H-6	H-7	H-7′
Heptose	$J_{H,H}$	$J_{1,2}$	$J_{2,3}$	$J_{3,4}$	$J_{4,5}$	$J_{5,6}$	$J_{6,7}$	$J_{6,7'}$	$J_{7,7'}$
D-α-L-		95.00[a]	71.45	71.36	67.05	71.81	69.63	63.84	
		5.166	3.914	3.838	3.845	3.749	4.024	3.689	3.652
		1.8	3.1	10.0	9.7	1.6	7.3	5.5	–11.7
D-β-L-		94.74[b]	72.02	74.09	66.69	75.43	69.53	63.57	
		4.866	3.927	3.649	3.788	3.329	3.98	3.713	3.695
		1.0	3.2	10.0	9.8	1.8	7.5	5.8	–11.7
D-α-D-		94.86[a]	71.32	71.38	68.35	73.42	72.72	62.75	
		5.151	3.905	3.812	3.756	3.865	4.018	3.797	3.708
		1.8	3.4	9.4	10.1	3.2	3.3	7.6	–12.0
D-β-D-		94.79[b]	71.84	74.11	68.16	77.22	72.623	62.58	
		4.851	3.921	3.622	3.682	3.423	4.025	3.788	3.725
		1.1	3.3	9.5	9.9	3.3	3.4	7.4	–12.0

Note: Measured at 600 MHz (^{1}H) in D_2O at 25°C from ^{1}H spin simulations and from the ^{13}C spectra (150 MHz) with the CH_3 signal of acetone set at 2.225 ppm for ^{1}H NMR and 31.07 ppm for ^{13}C NMR. δ_C and δ_H are in ppm with an average error of ±0.005 ppm for δ_C and ±0.003 ppm for δ_H. $J_{H,H}$ values are in Hz with an average error of ±0.2 Hz. H-7 and H-7′ are in decreasing g order of chemical shifts.
[a] $J_{C1,H1}$ = 171 ± 1 Hz.
[b] $J_{C1,H1}$ = 160 ± 1 Hz measured from the undecoupled ^{13}C NMR spectrum.

Fig. 6. Proton spectra of heptose monosaccharides. Resolution enhanced spectrum of D-L-heptose at 600 MHz in D_2O, 300 K (*a*) and its simulated spectrum for the α (*b*) and β forms (*c*). Resolution enhanced spectrum of D-D-heptose at 600 MHz in D_2O, 300 K (*d*) and its spin simulated spectra for the α (*e*) and β forms (*f*). The anomerics and H-5β resonances are not shown. Note that strong coupling for the H-3, H-4 and virtual coupling for H-5 resonances are reproduced correctly for (*b*).

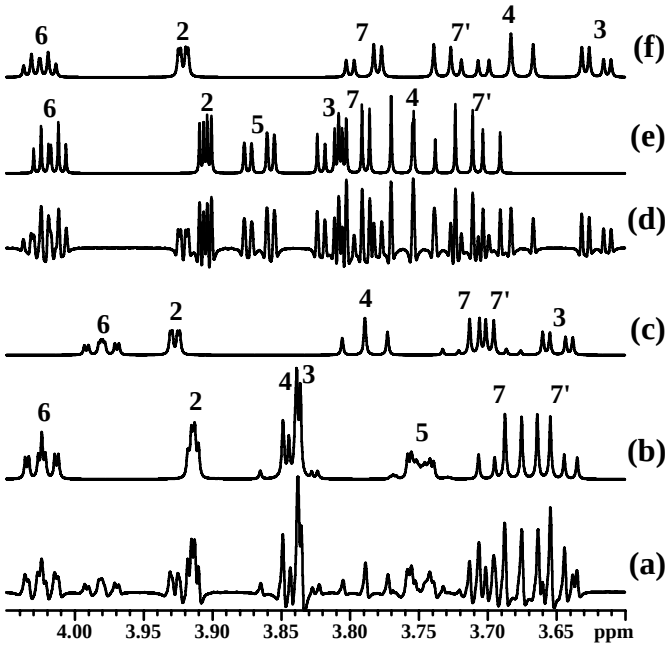

the 1D-NOESY for i1 (Fig. 5*f*). In the HMQC spectrum two narrow crosspeaks at (δc, δh) (74.9, 4.17), (72.5, 4.17) and a broader one at (75.3, 4.01) were identified. HMQC-TOCSY correlations were also observed between these crosspeaks. From a comparison of the ^{13}C NMR chemical shifts with those of the α-D-heptopyranoses in Table 2, it was obvious that the crosspeaks at (74.9, 4.17) and (75.3, 4.01) were subject to a ^{13}C NMR down-field glycosidation shift. Since these three crosspeaks are from d3, d4, or d5, only the d5 crosspeak will not experience a large glycosidation shift since substitutions on heptose cannot occur at C-5. Hence, the crosspeak at (72.5, 4.17) was assigned to (C-5, H-5). The crosspeak at (75.3, 4.01) was assigned to (C-3, H-3) based on the HMBC (d3, d1) and (d3, b1) correlations. The crosspeak at (74.9, 4.01) was thus assigned as (d4, d1), consistent with the observation of the HMBC (d4, i1) correlation and (i1, d4) NOE (Fig. 3 and Fig. 5*f*). The d6 resonance was assigned from the 1D-NOESY from i1, since for the Glc_I-(1-4)-Hep_I linkage, a strong NOE to H-6 is also expected only if residue **d** is L-D-heptose. The d6 resonance was also observed for the 1D-NOESY for c1 (Fig. 5*b*). The H-7 and H-7′ resonances were located from the HMQC-TOCSY (C-7, H-6) crosspeak (Fig. 3) and from 1D-NOESY-TOCSY (i1, d6) (not shown). Comparison of chemical shifts with those of L-α-D-heptose indicated a 3.9, 7.9, and 11.6 ppm down-field glycosidation shift for C-3, C-4, and C-6, respectively.

As shown below, there should be a 4,6-disubstituted L-α-D-heptose (**d′**) present due to heterogeneity on the branching heptose (Fig. 1). From the HMQC and COSY spectra for the anomeric region, no separate signal could be observed either for the H-1 or H-2 due to overlap with other resonances. It is suspected that the proton chemical shifts of d′1 were the same as the one for d1, and that d′2 had a similar chemical shift to e2.

Residue **g** was determined to be a 6-substituted D-α-D-heptose denoted as Hep_{IV}. The 1D-TOCSY-TOCSY (g1, g2) identified the g3, g4, and g5 spins (Fig. 7*e*). The multiplet pattern at 3.94 was indicative of a H-5 resonance. To identify H-6, an 1D-TOCSY-NOESY (g2, g5) was acquired (Fig. 7*f*). NOEs from g2 were observed on g3 and g6 along with a putative inter-residue NOE on i6. Once g6 was located, the HMQC-TOCSY from the C-7-H-7s-C-6-H-6 (Fig. 3*b*) and 1D-NOESY-TOCSY (f1, g6) (Fig. 7*g*) were

Fig. 7. 1D selective experiments for assignment of the heptose residues in A1. (*a*) 1D TOCSY-TOCSY (b1, 75 ms; b2, 75 ms) to detect b3, b4 and b5; (*b*) 1D TOCSY-NOESY (b2, 150 ms; b5, 400 ms) to detect the b5-b6 and b5-b3 NOEs. Note also the strong b5-d2 NOE due to the b(1-3)d linkage; (*c*) 1D TOCSY-TOCSY (de1, 75 ms; e2, 75 ms) to detect e3, e4 and e5; (*d*) 1D TOCSY-TOCSY (de1, 75 ms; d2, 75 ms) to detect d3, d4 and d5; (*e*) 1D TOCSY-TOCSY (g1, 90 ms; g2, 150 ms) to detect g3 to g5; (*f*) 1D TOCSY-NOESY (g2, 150 ms; g5, 400 ms) showing the g5-g6 and g5-g3 NOEs and g5-i6 NOE in accord with the g(1-6)i linkage; (*g*) 1D NOESY-TOCSY (f1, 400 ms; g6 180 ms) to detect the g7 resonances from the f1-g6 interglycosidic NOE in accord with the f(1-6)g linkage; (*h*) 1D TOCSY-TOCSY (f1, 90 ms; f2, 150 ms) for detection of f and f′ resonances up to H-6. Note the clear multiplet pattern for f5 and f′5; (*i*) 1D TOCSY (f6, 40 ms) to detect the f7 resonances only due to the short spin lock time. The resonance for the first selective step is underlined and the one for second selection step is doubly underlined, where applicable. Selected resonances in the anomeric region are indicated on the left of the spectra.

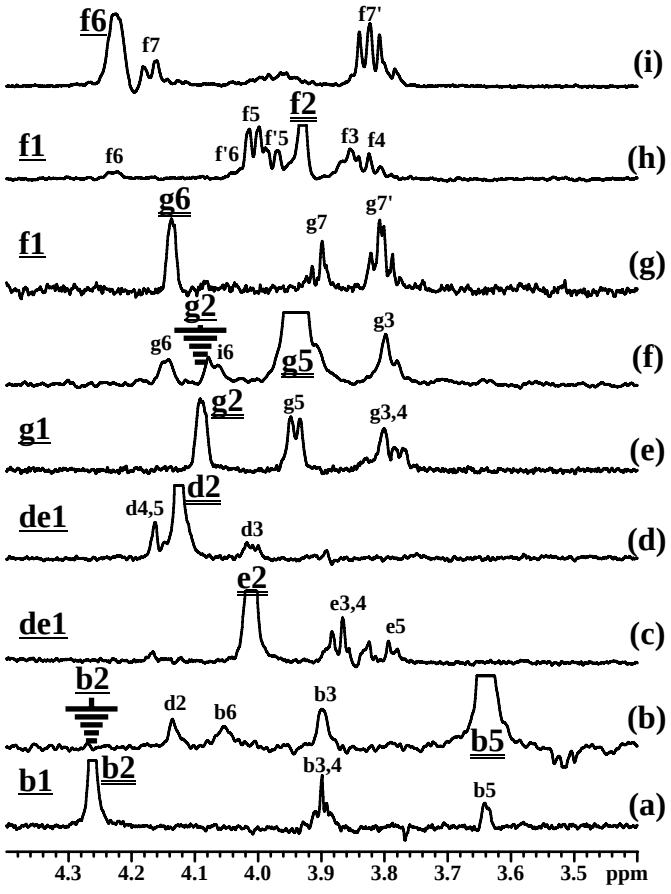

used to assign the H-7 and H-7′ resonances. Assignments for the other resonances were then obtained from the HMQC spectrum and confirmed with the HMQC-TOCSY spectrum (Fig. 3). In the 1D-NOESY (f1), the g6 and g5 resonances were observed (Fig. 5*d*). The NOE f1-g5 NOE can only be possible if residue **g** is a D-D-heptose from molecular modeling studies (see below). Comparison of chemical shifts with those of D-α-D-heptose indicated a 4.3 ppm down-field shift for C-6.

Residue **f** was determined to be a 7-substituted D-α-D-heptose and denoted as Hep_V. The 1D-TOCSY-TOCSY (f1, f2) identified spins up to f6 indicating that residue **f** was a D-D-heptose. The f5 multiplet pattern was quite clear. From a 1D-TOCSY starting on f6, the f7, and f7′ resonances were identified. The ^{13}C NMR assignments were then obtained from the HMQC spectrum and confirmed with the HMQC-TOCSY spectrum. Comparison of chemical shifts with those of α-D-D-heptose indicated a 8.8 ppm down-field shift for C-7. A terminal D-α-D-heptose, denoted **f′**, was only detected due to heterogeneity at this linkage site. As seen in the 1D-TOCSY-TOCSY (f1, f2), the f′5 and f′6 resonance can be detected, along with crosspeaks in the HMQC and HMQC-TOCSY spectra which correspond to those of a terminal D-α-D-heptose similar to those for D-α-D-heptose in Table 2.

The sequence of the core octasaccharide was established from the 1D-NOESY spectrum for the anomeric resonances presented in Fig. 5 and from the HMBC spectrum of the anomeric proton resonances (Fig. 3*c*). Inter-residue NOEs were also observed in 1D-TOCSY-NOESY experiments in Fig. 7*b* and 7*f*. The results are tabulated in Table 3 and the structure shown in Fig. 1. From integration of the anomeric resonances and appearance of new resonances with time, the linkage sites where heterogeneity occurs were determined. The k(2-6)h linkage and the b(1-3)d linkage hydrolyzed over a period of months in solution at pH 3, while the j(1-7)f linkage was stable.

An unusually large number of long-range NOEs were observed spanning up to five sequential residues. For an α-D sugar, the H-1-H-2 intra-residue NOE is expected. For a β-D sugar, the H-1-H-3 and H-1-H-5 intra-residue NOEs are expected. The H-1-C-1-O-1-C-*x*-H-*x* interglycosidic NOEs are expected for (1-*x*) linkage. Inter-residue anomeric NOEs between two linked sugars on the H-*x* ± 1 and H-*x* ± 2 can also occur. Other inter-residue NOEs, not in the vicinity of the glycosidic linkage, are deemed to be long-range NOEs as listed in Table 3.

To explain the large number of long-range NOEs, conformational analysis was done using the Metropolis Monte Carlo (MMC) method to vary the glycosidic linkage angles and sample the multiple conformations of the molecule. Using this method for the inner core oligosaccharide with Kdo at the reducing end, it was found that all the observed long-range NOEs could be explained by the close proximity of the e-b branch to the g-i branch. These long-range NOEs were possible due to restriction of the inner core residues brought about by the three branching points on Hep_I.

A minimum energy conformer obtained from the calculation is shown in Fig. 8. The various interproton distances measured from these coordinates are given in Table 3. As can be observed the occurrence of most NOEs can be explained by the short inter-proton distances. The long-range NOEs for g1-b2 and g1-b3 are not consistent with distances obtained from the molecular model drawn in Fig. 8. Although there is restriction due to the 3,4,6)-Hep_I substitution pattern, there is flexibility about the glycosidic linkage and this must be taken into account. As shown in Fig. 9 for the g1-b2 and g1-b3 distances, multiple conformations having short inter-proton distances are sampled consistent with the observed NOEs. The same situation was applicable for all

Table 3. HMBC and NOE data for A1 and distances from a minimum energy conformer of the core heptasaccharide shown in Fig. 8.

Linkage	HMBC H-1-C-*x*	Intra-residue NOE	*r* (Å)	Inter-residue NOE	*r* (Å)	Long range NOE	*r* (Å)
b(1-3)d	b1-d3	b1-b2	2.6	b1-d3	2.6	b1-e5	3.3
		b5-b3	2.5	b1-d4	3.7	b1-e7	2.9
		b5-b6	2.4	b5-d2	2.3	b1-e7′	2.6
				k3ax-d5	3.2	b1-i2	2.2
c(1-6)d	c1-d6	c1-c2	2.4	c1-d6	2.0	c1-i1	2.4
d(1-5)k		d1-d2	2.6	d1-k5	2.2		
				d1-k7	2.9		
e(1-2)b	e1-b2	e1-e2	2.6	e1-b2	2.1	e1-g2	4.2
				e1-b1	2.8	e1-g3	2.3
						e1-i4	2.0
f(1-6)g[a]	f1-g6	f1-f2	2.6	f1-g6	2.5		
				f1-g5	2.6		
g(1-6)i	g1-i6	g1-g2	2.6	g1-i6	2.6	g1-b2	4.2
		g5-g3	2.6	g1-i6′	2.6	g1-b3	4.9
		g5-g6	2.5	g5-i6	3.0		
i(1-4)d	i1-d4	i1-i3	2.6	i1-d4	2.8	i1-c1	2.4
		i1-i5	2.4	i1-d6	2.1		
j(1-7)f[a]	j1-f7	j1-j2	3.1	j1-f7	2.7		
		j1-j3	2.7	j1-f7′	2.5		
		j1-j5	2.4				

[a]For the j and f residues in the Gal-(1-7)-Hep_V-(1-6)-Hep_{IV} sequence (j-f-g), the average distances from MMC calculations are given.

Fig. 8. Molecular model of a minimum-energy conformer obtained from a MMC calculation of the inner core heptasaccharide of A1. Oxygens are depicted as the larger spheres and hydroxyl protons are removed. Relevant protons are labelled. Note the close proximity of the e-b branch to the g-i branch and the close proximity of the exocyclic chain of residue **e** to the anomeric proton of residue **b** consistent with the long range NOEs observed. Also, note the differences in orientation of the exocyclic chain between L-D heptose (residues **d**, **b**, **e**) and D-D heptose (residue g).

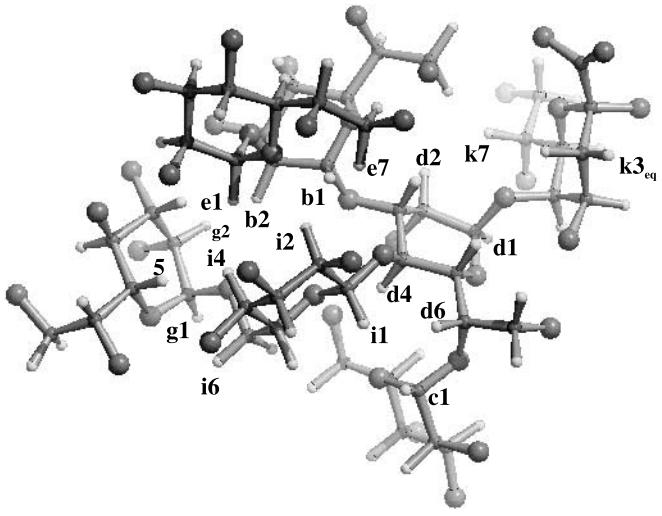

the other long-range and inter-residue NOEs. The long-range NOEs for g1-b2 and g1-b3 and e1-i4 span four residues with mobility about the three glycosidic (ϕ, ψ) angles for a total of 6 df. The long-range NOEs between e1-g2 and e1-g3 that span five residues (e-b-d-i-g) vary even more due to 8 df

Fig. 9. Variation of inter-proton distances (*r*) vs. macro move in a MMC calculation of the inner core heptasaccharide of A1 for b1-e5, b1-e7, e1-i4, e1-g2, g1-b2, g1-b3 in (a)–(g), respectively. Occurrences of interproton distances in the 2–4 Å range are consistent with the observed long range b-e, e-i, and e-g NOEs.

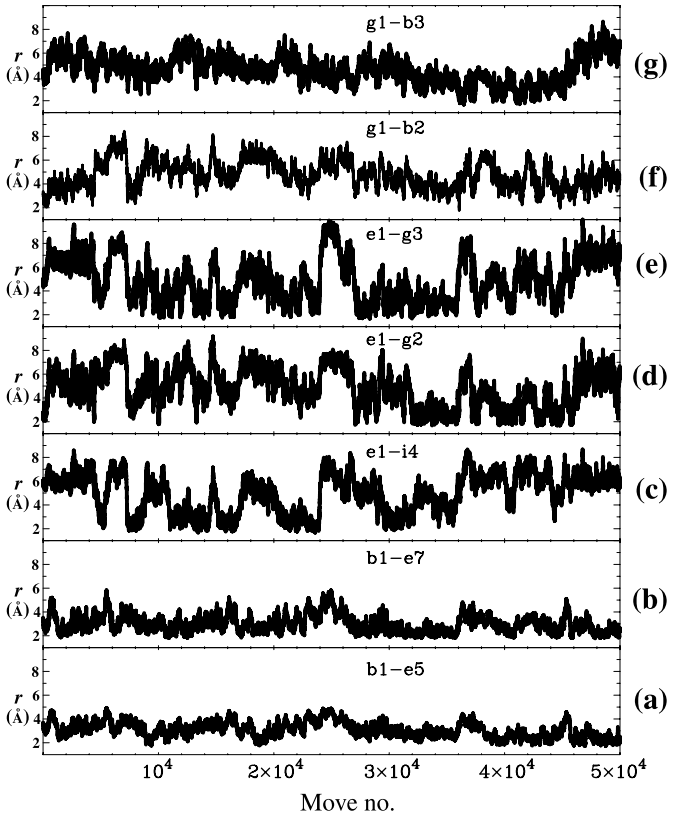

about the glycosidic angles, not counting possible flexibility about the C-5—C-6 bond for the g(1-6)i linkage. The b1-e5, b1-e7, and b1-e7′ are dependent on mobility about the e(1-2)b glycosidic bond and rotation about C-6-C-7 of residue **e**. In all cases, the occurrence of multiple conformations that have short inter-proton distances is consistent with the observed inter-residue and long-range NOEs.

In the present study it was established that the lipid A region of the *M. haemolytica* A1 LPS molecule contains a bis-4,4′-phosphorylated β-1,6 linked D-glucosamine disaccharide moiety. The nature and substitution patterns of the fatty acyl groups attached to this disaccharide have not been reported. The fully acylated LPS molecule makes up the outer most leaflet of the bacterial membrane and is essential for maintaining membrane integrity. The glycose portion of the molecule typically extends out and away from the plane defined by the bacterial membrane. The LPS oligosaccharide portion is important in virulence (70) and is involved in eliciting host immune responses (17). To gain a perspective of the relative sizes and orientation of the core oligosaccharide and membrane-anchoring lipid A regions of this LPS molecule, a molecular model was constructed using the lipid A fatty acid substitution pattern found in a related organism, *Haemophilus influenzae*. This is shown in Fig. 10. The *H. influenzae* lipid A has been reported (71) to have six fatty acyl groups in which the amide group (C-2) and C-3 hydroxyl groups of the reducing glucosamine residue are acylated by 3-hydroxytetradecanoic acid while the C-2′ amide and C-3′ hydroxyl groups of the nonreducing residue are acylated by 3-tetradecanoyloxytetradecanoic acid.[2] As observed in Fig. 10, due to the inner core which provides a fairly rigid structure, the glycose portion projects out from the lipid A moiety which defines the bacterial membrane. More mobility was observed for the terminal residues, especially for the terminal Gal residue. In the NOESY spectrum in Fig. 2, no NOEs for the anomeric resonance were observed consistent with increased mobility of this residue.

The core structures of several LPS have been found to be highly branched (3) and this can result in well-defined conformations for the inner core. In a previous study, the LPS of *Moraxella catharrhalis* was found to adopt an unusual conformation in which a very rare *anti* conformer (72) was observed (73). For a highly branched 3,4,6-trisubstituted D-glucose residue in this LPS molecule, a dihedral angle (C-1′-O-1′-C-4-H-4) near 180° was detected for β-D-Glc*p*-(1–4)-D-Glc*p* linkage to the branched glucose unit.

The results of the present study have provided a detailed picture of the structure of the LPS core oligosaccharide region of *M. haemolytica* serotype A1. We have previously shown that the oligosaccharide region of *M. haemolytica* LPS is immunogenic in mice, sheep, and cattle and that eight of the 12 *M. haemolytica* serotypes (i.e., serotypes A1, A5, A6, A7, A8, A12, A14, and A16) share common core oligosaccharide determinants (17). The core oligosaccharides from serotypes A1 and A8 show almost identical ^{1}H NMR spectra (17) establishing the presence of a common basal structure. Based on the results of the present study it is apparent that the *O*-chain deficient LPS elaborated by *M. haemolytica* serotype A8 lacks the terminal Gal unit in the core oligosaccharide, a residue which possibly provides a site for *O*-chain attachment (16). An understanding of LPS structural differences among *M. haemolytica* serotypes could provide the basis for a vaccine against *M. haemolytica* bovine pasturellosis. Serotype A1 is the principal microorganism responsible for this disease, accounting for 30% of total cattle deaths globally (11). The use of a less virulent serotype or antigens thereof in a vaccine formulation could provide an effective disease management strategy.

Experimental

Preparation of LPS from *M. haemolytica*

Pasteurella (Mannheimia) haemolytica serotype A1 (NRCC 4212) was obtained from the Veterinary Infectious Diseases Organization (VIDO), Saskatoon, SK, Canada. LPS was extracted and purified from fermenter-grown bacteria culture by the hot aqueous phenol method as previously described (16).

Deacylation of LPS to give backbone oligosaccharides

Backbone oligosaccharide was prepared as previously described (74) by modification of the deacylation procedure of Holst et al. (75). Ester-bound fatty acids were removed from the lipid A of the LPS by treatment of a sample (400 mg) with anhydrous hydrazine at ambient temperature (20 mL, 37°C, 30 min). Excess hydrazine was destroyed by addition of acetone (three volumes) to the cooled reaction mixture (0°C). The precipitated *O*-deacylated LPS product was isolated by centrifugation (5000 rpm, 10 min), washed with acetone, and lyophylized from water. Removal of *N*-acyl groups was achieved by heating the *O*-deacylated sample (200 mg) in aq KOH (4 M, 10 mL) at 100°C for 20 h. The reaction mixture was cooled (0°C), neutralized with 4 M HCl, and the precipitated fatty acids removed by centrifugation (12 000 × g, 30 min). The supernatants were filtered in an Amicon concentration cell with a 500-molecular-weight-cutoff membrane (Amicon; YC05) and washed with deionized water until the eluant was free of chloride ions (as determined with aq $AgNO_3$). The dialyzed material was lyophylized to give deacylated LPS (ca. 80 mg). The oligosaccharide was purified by anion-exchange chromatography on DEAE A-25 (74). The backbone oligosaccharide fraction (ca. 50 mg) showed a doubly charged ion at *m*/*z* 1124.8 in the positive ion ESI-MS as the major ion which corresponded to a composition of Hex_3Hep_5 Kdo $HexN_2(H_2PO_3)_3$ (M, 2246.9). MS–MS of the doubly charged ion gave characteristic fragments at *m*/*z* 500 ($HexN_2(H_2PO_3)_2$) and 801 ($KdoHexN_2(H_2\ PO_3)_2$) corresponding to deacylated lipid A and the Kdo-P substituted units, respectively.

D-glycero-L-manno-*Heptose*

The heptose was prepared by the condensation of D-galactose with nitromethane in alkaline methanol (76). The crystalline 1-deoxy-1-nitro-D-*glycero*-L-*manno*-heptitol obtained from the aqueous solution of the deionized products (mp

[2] ES-MS of O-deacylated LPS from *M. heamolytica* serotype A1 is consistant with each glucosamine residue containing an amide-linked 3-hydroxytetradecanoic acid group (data not shown).

Fig. 10. Molecular model of the LPS of *M. haemolytica* A1 constructed using a lipid A having the fatty acyl substitution patterns reported (71) for LPS from *H. influenzae*. The lipid A moiety is colored with the atoms C in black, O in red, and H in white. The sugar moiety is colored with Kdo in gray, heptoses in red or purple, glucose in green, and galactose in blue. The PO_4 groups are yellow. Hydroxyl protons have been removed.

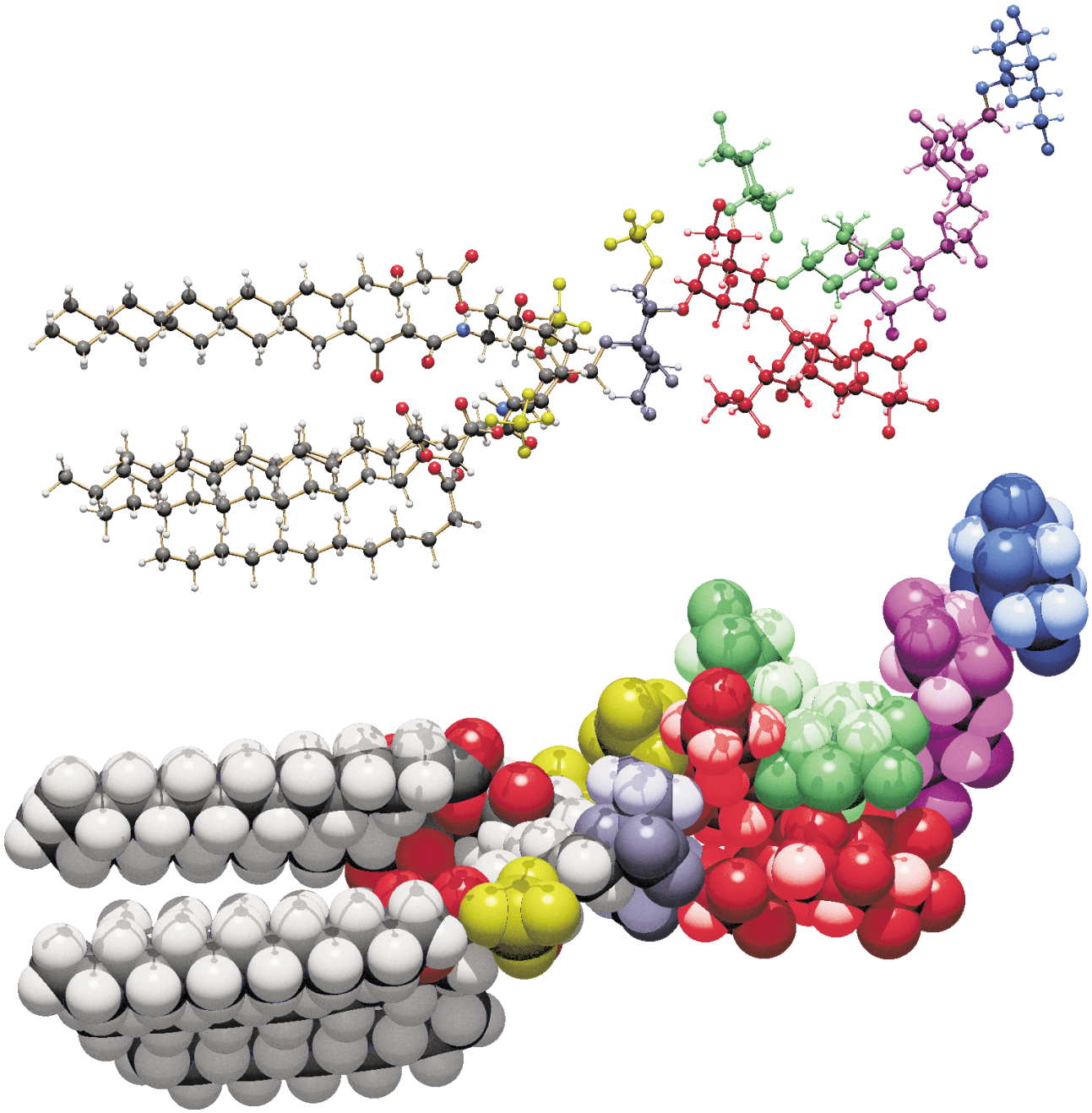

158°C, 21% yield) was converted to its sodium salt. On treatment with dilute sulphuric acid (35°C), followed by deionization with Rexyn 101(H^+) and Amberlite A4(OH^-) ion-exchange resins, the solution was lyophilized to give the heptose as a syrup (80% yield). The product was fractionated by cellulose column chromatography using butan-1-ol–water (1:10 v/v) as the eluant. Fractions containing the heptose were concentrated to dryness under reduced pressure. The D-*glycero*-L-*manno*-heptose having $[\alpha]_D$ –14° (*c* 0.2, water) was pure by paper chromatography and its reduced ($NaBH_4$) and acetylated product on GLC gave a single peak corresponding in retention time with that of authentic hepta-*O*-acetyl-D-*glycero*-L-*manno*-heptitol, establishing its purity.

D-glycero-D-manno-*Heptose*

The heptose was prepared from D-altrose via its condensation with nitromethane to yield 1-deoxy-1-nitro-D-*glycero*-D-*manno*-heptitol (mp 109°C, $[\alpha]_D$ –7.0° (*c* 1.1, EtOH), 27% yield)) whose aqueous sodium salt solution on slow dropwise addition to stirred 20% (v/v) sulfuric acid maintained at 0°C

was converted to D-*glycero*-D-*manno*-heptose (77). The reaction mixture was neutralized with sat. $Ba(OH)_2$ solution, filtered, passed through Rexyn 101(H^+) and Duolite A4(OH^-) ion-exchange resins to remove residual ionic material, and was concentrated to a syrup (92% yield). The heptose product, as indicated by paper chromatography, was contaminated with altrose and unchanged 1-deoxy-1-nitro-D-*glycero*-D-manno-heptitol (ca. 2 to 3%). The product was purified by cellulose column chromatography using butan-1-ol–water (1:10 v/v) as the mobile phase. The D-*glycero*-D-*manno*-mannose had $[\alpha]_D$ +22° (*c* 2, MeOH). A reduced ($NaBH_4$) and acetylated sample on GLC gave a single peak corresponding to authentic hepta-*O*-acetyl-D-*glycero*-D-*manno*-D-heptitol indicating the identity and purity of the synthesized heptose.

Electrospray mass spectrometry

Samples were analyzed on a VG Quattro triple quadrupole mass spectrometer (Micromass, Manchester, U.K.) fitted with an electrospray ion source. Backbone oligosaccharide was dissolved in acetonitrile–water (approx. 1:2 v/v) containing 0.5% acetic acid. Injection volumes were 10 μL and the flow rate was set at 4 mL min^{-1}. The electrospray tip voltage was typically 2.7 kV and the mass spectrometer was scanned from *m*/*z* 50 to 2500 with a scan time of 10 s. For MS–MS experiments, precursor ions were selected using the first quadrupole and fragment ions formed by collisional activation with argon in the RF-only quadrupole cell, were mass analyzed by scanning the third quadrupole. Collision energies were typically 60 ev (laboratory frame of reference).

Nuclear magnetic resonance

NMR spectra were performed on a Bruker AMX 600, AMX 500, or a Varian Inova 600 spectrometer using standard software. All measurements were made at 300 K and at pH 3, containing 10 mg of sample dissolved in 0.6 mL of D_2O. Measurements were done at pH 3 to improve resolution of the proton spectrum as done previously (65). Acetone was used as an internal or external reference at 2.225 ppm for ^1H spectra and 31.07 ppm for ^{13}C spectra. Standard homo- and heteronuclear correlated 2D techniques were used for general assignments of the core oligosaccharide: COSY, TOCSY, NOESY, triple quantum homonuclear correlated experiment, HMQC, HMQC-TOCSY, and HMBC and ^{31}P HMQC (78). Spin simulations for the heptose monosaccharides were performed with standard Varian software. Accurate chemical shifts and coupling constants were obtained from the parameters used to perform the spin simulation and not from the peak listing of the spectra.

Selective 1D-TOCSY, 1D-NOESY, 1D-TOCSY-TOCSY, 1D-TOCSY-NOESY, and 1D-NOESY-TOCSY experiments were performed for complete residue assignment and for determination of inter-residue ^1H-^1H nuclear Overhauser enhancements. The nomenclature used to describe the use of the 1D selective sequences will be 1D EXP (spin, mixing time) and 1D EXP1-EPX2 (spin1, mixing time; spin2, mixing time), where EXP, EXP1, and EXP2 stand for either TOCSY or NOESY. Also, in the figures, the selected resonances are underlined. A doubly underlined resonance means that this resonance was selected as the second selection step. As shown in Fig. 1, all the residues are labeled by letters and the spins are labeled by the atom number, so that a1 refers to the H-1 resonance of residue **a**.

On the AMX spectrometers, selective excitation was achieved by means of half-Gaussian pulses. The mixing time used for a TOCSY depended on the spin system. Usually a range of mixing times (spin lock times) from 30 to 180 ms was used to assign the spin system. The mixing time for a 1D-NOESY depended on the correlation time of the molecule and internal motion about the glycosidic linkage. NOESY mixing times were in the range from 150 to 400 ms. To detect inter-residue NOEs for the terminal Gal residue, a 1D-ROESY experiment was done with a mixing time of 500 ms. For the doubly selective experiments, the selective pulses were kept as short as possible to avoid loss of signal intensity due to relaxation effects. Each part was optimized one at a time. The 1D-TOCSY could be carried out in a matter of minutes. The 1D-NOESY took from minutes to hours depending on the magnitude of the NOE. Some doubly selective experiments took up to 12 h. The 1D-TOCSY-TOCSY and 1D-TOCSY-NOESY were the most efficient. As the sample degraded with time, some experiments were also performed on an Inova 600 spectrometer making use of pulse field gradients.

Molecular modeling

The conformational analysis was done using the Metropolis Monte Carlo method as previously described (79). The PFOS potential was used (80). Minimized coordinates for the monosaccharides were obtained using MM3 (92) available from the Quantum Chemistry Program Exchange (QCPE). The minimum energy conformation for each disaccharide was used as the starting conformation. Starting from the Kdo at the reducing end, calculations were performed for various oligosaccharides up to the complete structure. For the inner core octasaccharide, 5×10^4 macro moves were used with a step length of 5° for the glycosidic linkage and a temperature of 1×10^3 K resulting in an acceptance ratio of 0.36. The molecular model for the inner core octasaccharide was generated using the minimum energy conformer. Distances were extracted from the saved coordinates at each macro move. The complete LPS with lipid A was generated using the lipid A structure (81) and the minimum energy conformer for the Kdo linkage. Molecular drawings were done using Schakal97 from E. Keeler, University of Freiburg, Germany.

Acknowledgements

We thank D.W. Griffith for large-scale production of cells and D. Krajcarski for ESI-MS analyses.

References

1. E.Th. Rietschel, L. Brade, U. Schade, U. Seydel, U. Zähringer, S. Kusmoto, and H. Brade. Bacterial endotoxins: properties and structure of biologically active domains, in surface structures of microorganisms and their interactions with the mammalian host. *In* Proceedings Workshop Conference, Hoechst, Verlag Chemie. *Edited by* E. Schrinner, M.H. Richmond, G. Seibert, and U. Schwarz. Weinheim, Germany. 1988. p. 1.

2. C.R.H. Raetz. Annu. Rev. Biochem. **59**, 129 (1990).
3. O. Holst and H. Brade. Chemical structure of the core region of lipopolysaccharides. *In* Bacterial endotoxic lipopolysaccharides. *Edited by* D.C. Morrison and J.L. Ryan. CRC Press. Boca Raton, Fla. 1992. p. 135.
4. S. Pohl. DNA relatedness among members of *haemophilus, pasteurella* and *actinobacillus. Haemophilus, pasteurella* and *actinobacillus. Edited by* M. Kilian, W. Frederiksen, and E.L. Biberstein. Academic Press. New York. 1981. p. 245.
5. E.L. Biberstein. Biotyping and serotyping of *Pasteurella haemolytica*. *In* Methods in enzymology. *Edited by* T. Bergan and J.R. Norris. Academic Press. New York. 1978. p. 253.
6. M. Younan and L. Fodor. Res. Vet. Sci. **58**, 98 (1995).
7. G.R. Smith. J. Pathol. Bacteriol. **81**, 431 (1961).
8. D.P. Bingham, R. Moore, and A.B. Richards. Am. J. Vet. Res. **51**, 1161 (1990).
9. P.H.A. Sneath and M. Stevens. Nov. Int. J. Syst. Bacteriol. **40**, 148 (1990).
10. O. Angen, M. Quirie, M. Donachie, and M. Bisgaard. Vet. Microbiol. **65**, 283 (1999).
11. D. Griffin. *In* Veterinary clinics of North America: Food animal practice. *Edited by* J. Vestweber and G. St Jean. Philadelphia. 1997. p. 367.
12. W.D.G. Yates. Can. J. Comp. Med. **46**, 225 (1982).
13. A.W. Confer, K.D. Clinkenbeard, and G.L. Murphy. Pathogenesis and virulence of *Pasteurella haemolytica* in cattle: an analysis of current knowledge and future approaches. *In Haemophilus, actinobaccilus* and *pasteurella. Edited by* W. Donachie, F.A. Lainson, and J.C. Hodgson. Plenum Press. New York. 1995. p. 51.
14. M.A. Breider, S. Kumar, and R. Corstvet. Vet. Immuno. Immunopathol. **27**, 337 (1991).
15. D.B. Paulsen, D.A. Mosier, K.D. Clinkenbeard, and A.W. Confer. Am. J. Vet. Res. **50**, 1633 (1989).
16. W.B. Severn and J.C. Richards. Carbohydr. Res. **240**, 277 (1993).
17. R.P. Lacroix, J.R. Duncan, R.P. Jenkins, R.A. Leitch, J.A. Perry, and J.C. Richards. Infect. Immun. **61**, 170 (1993).
18. M.B. Perry and L.A. Babiuk. Can. J. Biochem. Cell Biol. **62**, 108 (1984).
19. R.A. Leitch and J.C. Richards. Can. J. Biochem. Cell Biol. **66**, 1055 (1988).
20. J.C. Richards and R.A. Leitch. Carbohydr. Res. **186**, 275 (1989).
21. R.U. Lemieux and K. Bock. Arch. Biochem. Biophys. **221**, 125 (1983).
22. R.U. Lemieux. Chem. Soc. Rev. **18**, 347 (1989).
23. D.W. Hood, A.D. Cox, M. Gilbert, K. Makepeace, S. Walsh, M.E. Deadman, A. Cody, A. Martin, M. Mansson, E.K. Schweda, J.R. Brisson, J.C. Richards, E.R. Moxon, and W.W. Wakarchuk. Mol. Microbiol. **39**, 341 (2001).
24. E.H. Schweda, J.R. Brisson, G. Alvelius, A. Martin, J.N. Weiser, D.W. Hood, E.R. Moxon, and J.C. Richards. Eur. J. Biochem. **267**, 3902 (2000).
25. I. Sadovskaya, J.R. Brisson, P. Thibault, J.C. Richards, J.S. Lam, and E. Altman. Eur. J. Biochem. **267**, 1640 (2000).
26. J.S. Plested, K. Makepeace, M.P. Jennings, M.A. Gidney, S. Lacelle, J.R. Brisson, A.D. Cox, A. Martin, A.G. Bird, J.C. Tang, J.C. Richards, and E.R. Moxon. Infect. Immun. **67**, 5417 (1999).
27. W.W. Wakarchuk, M. Gilbert, A. Martin, Y. Wu, J.R. Brisson, P. Thibault, and J.C. Richards. Eur. J. Biochem. **254**, 626 (1998).
28. A.D. Cox, M.D. Howard, J.R. Brisson, M. van der Zwan, P. Thibault, M.B. Perry, and T.J. Inzana. Eur. J. Biochem. **253**, 507 (1998).
29. D.G. Davis and A. Bax. J. Am. Chem. Soc. **107**, 9197 (1985).
30. H. Kessler, H. Oschkinat, and C. Griesinger. J. Magn. Reson. **70**, 106 (1986).
31. H. Kessler, U. Anders, G. Gemmecker, and S. Steuernagel. J. Magn. Reson. **85**, 1 (1989).
32. L.D. Hall and T.J. Norwood. J. Magn. Reson. **87**, 331 (1990).
33. J. Friedrich, S. Davies, and R. Freeman. J. Magn. Reson. **80**, 168 (1988).
34. E. Kupce and R. Freeman. J. Magn. Reson. **100**, 208 (1992).
35. X.J. Miao and R. Freeman. J. Magn. Reson. **119**, 145 (1996).
36. R. Bazzo, C.J. Edge, R.A. Dwek, and T.W. Rademacher. J. Magn. Reson. **86**, 199 (1990).
37. D. Boudot, C. Roumestand, F. Toma, and D. Canet. J. Magn. Reson. **90**, 221 (1990).
38. L. Poppe and H. van Halbeek. J. Magn. Reson. **96**, 185 (1992).
39. D. Uhrín, J.R. Brisson, and D.R. Bundle. J. Biomol. NMR, **3**, 367 (1993).
40. S. Holmbeck, P.J. Hajduk, and L. Lerner. J. Magn. Reson. B, **102**, 107 (1993).
41. D. Uhrín, J.R. Brisson, G. Kogan, and H.J. Jennings. J. Magn. Reson. Ser. B, **104**, 289 (1994).
42. K. Zangger and H. Sterk. J. Magn. Reson. **107**, 186 (1995).
43. J. Stonehouse, P. Adell, J. Keeler, and A.J. Shaka. J. Am. Chem. Soc. **116**, 6037 (1994).
44. M.A. Bernstein and L.A. Trimble. Magn. Reson. Chem. **32**, 107 (1994).
45. P. Adell, T. Parella, F. Sanchez-Ferrando, and A. Virgili. J. Magn. Reson. Ser. A, **113**, 124 (1995).
46. C. Dalvit and G. Bovermann. Magn. Reson. Chem. **33**, 156 (1995).
47. T. Facke and S. Berger. J. Magn. Reson. Ser. A, **113**, 257 (1995).
48. C. Dalvit. J. Magn. Reson. **113**, 120 (1995).
49. P. Adell, T. Parella, F. Sanchez-Ferrando, and A. Virgili. J. Magn. Reson. Ser. B, **108**, 77 (1995).
50. T.L. Hwang and A.J. Shaka. J. Magn. Reson. **112**, 275 (1995).
51. K. Stott, J. Stonehouse, J. Keeler, T.L. Hwang, and A.J. Shaka. J. Am. Chem. Soc. **117**, 4199 (1995).
52. G. Xu and J.S. Evans. J. Magn. Reson. Ser. B, **111**, 183 (1996).
53. T. Parella. Magn. Reson. Chem. **34**, 329 (1996).
54. M.J. Gradwell, H. Kogelberg, and T.A. Frankiel. J. Magn. Reson. Ser. B, **124**, 267 (1997).
55. D. Uhrín and P.N. Barlow. J. Magn. Reson. **126**, 148 (1997).
56. W.W. Wakarchuk, D. Watson, F. St Michael, J. Li, Y. Wu, J.R. Brisson, N.M. Young, and M. Gilbert. J. Biol. Chem. **276**, 12 785 (2001).
57. M. Gilbert, J.R. Brisson, M.F. Kawarski, J. Michniewicz, A.M. Cunningham, Y. Wu, N.M. Young, and W.W. Wakarchuk. J. Biol. Chem. **275**, 3896 (2000).
58. J.R. Brisson, S. Uhrinova, R.J. Woods, M. van der Zwan, H.C. Jarrell, L.C. Paoletti, D.L. Kasper, and H.J. Jennings. Biochemistry, **36**, 3278 (1997).
59. K. Scheffler, J.R. Brisson, R. Weisemann, J.L. Magnani, T.C. Wong, B. Ernst, and T. Peters. J. Biomol. NMR, **9**, 423 (1997).
60. J.O. Duus, C.H. Gotfredsen, and K. Bock. Chem. Rev. **100**, 4589 (2000).
61. D. Uhrín and J.R. Brisson. Structure determination of microbial polysaccharides by high resolution NMR spectroscopy. *In* NMR in microbiology: theory and applications. *Edited by* J.N. Barbotin and J.C. Portais. Horizon Scientific Press. Wymondham, U.K. 2000. p. 165.
62. G. Kogan and D. Uhrín. Current NMR methods in the structural elucidation of polysaccharides. *In* New advances in analytical chemistry. *Edited by* Atta-ur-Rahman. Harwood Academic. Amsterdam. 2000. p. 73.

63. D. Uhrín. Concatenation of polarization transfer steps in 1D homonuclear chemical shift correlated experiments. Application to oligo- and polysaccharides. *In* Methods for structure elucidation by high-resolution NMR. *Edited by* Gy. Batta, K.E. Kövér, and C. Szántay, Jr. Elsevier Science B. V. Amsterdam. 1997. p. 51.
64. C. Roumestand, C. Delay, J.A. Gavin, and D. Canet. Magn. Reson. Chem. **37**, 451 (1999).
65. A.D. Cox, J.R. Brisson, V. Varma, and M.B. Perry. Carbohydr. Res. **290**, 43 (1996).
66. G.I. Birnbaum, R. Roy, J.R. Brisson, and H.J. Jennings. J. Carbohydr. Chem. **6**, 17 (1987).
67. E. Altman, J.R. Brisson, and M.B. Perry. Eur. J. Biochem. **170**, 185 (1987).
68. K. Bock and C. Pedersen. Adv. Carbohydr. Chem. Biochem. **41**, 27 (1983).
69. P.-E. Jansson, L. Kenne, and G. Widmalm. Carbohydr. Res. **188**, 169 (1989).
70. M.D. Potter and R.Y. Lo. FEMS Microbiol. Lett. **129**, 75 (1995).
71. I.M. Helander, B. Lindner, H. Brade, K. Altmann, A.A. Lindberg, E.T. Rietschel, and U. Zahringer. Eur. J. Biochem. **177**, 483 (1988).
72. S.A. Wacowich-Sgarbi, C.C. Ling, A. Otter, and D.R. Bundle. J. Am. Chem. Soc. **123**, 4362 (2001).
73. H. Masoud, M.B. Perry, J.R. Brisson, D. Uhrín, and J.C. Richards. Can. J. Chem. **72**, 1466 (1994).
74. W.B. Severn, R.F. Kelly, J.C. Richards, and C. Whitfield. J. Bacteriol. **178**, 1731 (1996).
75. O. Holst, U. Zahringer, H. Brade, and A. Zamojski. Carbohydr. Res. **215**, 323 (1991).
76. J.C. Sowden and D.R. Strobach. J. Am. Chem. Soc. **82**, 954 (1960).
77. R.K. Hulyalkar, J.K.N. Jones, and M.B. Perry. Can. J. Chem. **41**, 1490 (1963).
78. D. Uhrín, J.R. Brisson, L.L. MacLean, J.C. Richards, and M.B. Perry. J. Biomol. NMR, **4**, 615 (1994).
79. T. Peters, B. Meyer, P. Stuike, R. Somorjai, and J.R. Brisson. Carbohydr. Res. **238**, 49 (1993).
80. I. Tvaroska and S. Pérez. Carbohydr. Res. **149**, 389 (1986).
81. Y. Wang and R.I. Hollingsworth. Biochemistry, **35**, 5647 (1996).